Electronic SupplementaryInformation

Supporting $Cu@In_2O_3$ Core-Shell Structure on N-Doped Graphitic Carbon Cuboctahedra Cages for Efficient Photocatalytic Homo-Coupling of Terminal Alkynes

Yaya Yuan,†[a]Ya-QunWang,†[a]Guilin Zhuang,†[b] Qiuyan Li,[a] Feng-Lei Yang,*[a] XiaojunWang,[a] Xiguang Han*[a]

[a] *Jiangsu Key Laboratory of Green Synthetic Chemistry for Functional Materials, School of Chemistry and Material Science, Jiangsu Normal University, Xuzhou, 221116 (P. R. China) E-mail: yangfl@jsun.edu.cn; xghan@jsnu.edu.cn*

[b] *Laboratory of Molecular Catalysis &Computational Materials, Zhejiang University of Technology, Shanghai (P. R. China)*

† These authors contributed equally

Contents

1.Experiment Section

1.1 Synthesis of Cu-MOF-199 (HKUST-1)precursors

First, $Cu(NO_3)_2 \cdot 3H_2O$ (0.024 g, 0.1 mmol) was dissolved in the mixed-solvent of 4.5 mL ethanol and 4.5 mL N,N-dimethylformamide (DMF) to obtain solution (a). Then, benzimidazole (0.201g, 1.7 mmol) was added to the same mixed-solvent (4.5 mL ethanol and 4.5 mL DMF) to obtain solution (b). Solution (b) was added to solution (a) to form the bright blue solution (c), which was agitated for 10 min. 1,3,5-Benzenetricarboxylic acid (0.021 g, 0.1 mmol) was added to the mixed-solvent of 9 mL ethanol and 9 mL DMF to obtain solution (d). Solution (d) was added to solution (c) and agitated for 6 h at 90 °C. Finally, HKUST-1 was obtained by centrifuging, washing three times with anhydrous ethanol, and drying at 60 °C in an oven.

1.2 Synthesis of In-HKUST-1

In a typical synthesis, HKUST-1 (0.01 g), thiocarbamide (0.009 g, 0.12 mmol) and $In(NO_3)_3 \cdot 4H_2O$ (0.0186 g, 0.05 mmol) were dissolved in 5 mL DMF. The mixed solution was then transferred into a Teflon-lined stainless steel autoclave and heated at 120°C for 4 h. After the reaction, the product was collected by centrifugation, washed several times with anhydrous ethanol, and dried at 60°C in an oven.

1.3 Synthesis of Cu/In_2O_3@N-C Nanocomposites

Cu/In_2O_3@N-C nanoparticles were synthesized via calcination of the obtained In-HKUST-1 at 500 °C for 0.5 h in vacuum atmosphere with heating rate of 5 $°C \cdot min^{-1}$.

1.4 Synthesis of Cu@N-C Nanocomposites

Calcination of HKUST-1 at 500 °C for 0.5 h in vacuum atmosphere with heating rate of 5 $°C \cdot min^{-1}$.

1.5 Synthesis of Cu/In_2O_3 Nanocomposites

In-HKUST-1 were calcined at 500 °C for 2 h in oxygen atmosphere with heating rate of 2 $°C \cdot min^{-1}$. Then, Cu/In_2O_3 nanoparticles were synthesized via calcination for 4 h at 350 ^oC in H_2/Ar (H_2/Ar=10%) atmosphere.

1.6 Synthesis of In_2O_3@N-C Nanosheets

First, $In(NO_3)_3 \cdot 4H_2O$ (0.0186 g, 0.05 mmol), 1,3,5-Benzenetricarboxylic acid (0.021 g, 0.1 mmol) and benzimidazole (0.20 g, 1.7 mmol) were dissolved in 5 mL DMF agitated for 4 h at 120 °C. The product(In-MOF) was collected by centrifugation, washed several times with anhydrous ethanol, and dried at 60 °C. Then, In_2O_3@N-C nanosheets were synthesized via calcination of the product at 450 °C for 0.5 h in Ar atmosphere with heating rate of 5 $°C \cdot min^{-1}$.

1.7 Characterization

The composition and phase of the as-prepared products were acquired by the powder X-ray diffraction (XRD) pattern using a Panalytical X-pert diffractometer with CuKα radiation.The morphology and crystal structure of as-prepared products were observed by scanning electron microscopy (SEM, SU8010), and high-resolution transmission electron microscopy (HRTEM, FEI Tecnai-F20) with an acceleration voltage of 200 kV.All TEM samples were prepared from depositing a drop of diluted suspensions in ethanol on a carbon film coated copper grid.PHI QUANTUM2000 photoelectron spectrometer (XPS) was using to characterize the surface compositions of product.The surface areas of these samples were measured by the Brunauer-Emmett-Teller (BET) method using nitrogen adsorption and desorption isotherms on a Micrometrics ASAP 2020 system.Thermogravimentric analysis (TGA) was carried on a TGA-Q50 thermoanalyzer with a heating rate of 10 °C·min^{-1} under nitrogen atmosphere. Raman spectroscopy was measured using a Renishaw inVia 2000 Raman spectrometer and 532 nm excitation wavelength. The photoluminescence (PL) spectra was performed with an excitation wavelength of 250 nm.

1.8 Photoelectrochemical measurements

Photoelectrochemical experiments were measured in the three electrode quartz cell. The Pt plate was selected as the counter electrode, the reference electrode was Hg/$HgCl_2$ electrode, and the corresponding working electrode was obtained on the fluorine doped tin oxide (FTO) glass. In order to obtain a slurry, the obtained product (3 mg) was ultrasonicated in ethanol (0.1 mL). The slurry was then spread onto the FTO glass. The obtained working electrode with the area about 2.5 cm^2 was dried at 200 °C for 120 min. The CHI-760E workstation was used to measure the Electrochemical impedance spectra (EIS). In the three-electrode cell, the 0.025 M KH_2PO_4 and 0.025 M Na_2HPO_4 standard buffer solution (25 °C, pH=6.864) were selected as the electrolytes without adding any additive, and the measurements were performed on an open circuit potential condition. A 300 W Xe arc lamp system was used as the visible-light irradiation source. The linear sweep voltammetry (LSV) voltage was controlled in the range of -0.8~0.2 V, and the scanning speed was 0.01 V·s^{-1}. The photocurrent densities were measured under a potential of 0.3V.

1.9 Photocatalytic reactions

The catalyst (5 mg) and phenylacetylene (0.1mmol) were respectively added to acetonitrile (3 mL). The solution mixture was stirred and irradiated by blue LEDs (532 nm, 3 W) under air at room temperature. The yield of the product was characterized by ^{1}H NMR spectra. To perform the recycling experiments, the photocatalyst was recovered by centrifugation and washed with anhydrous ethanol for several times and then dried at 60°C in an oven.

2. Experiment Results

Fig. S1. (a) XRD pattern of the HKUST-1, (b) SEM image of the as-obtained HKUST-1,(c-f) EDX elemental mapping of Cu, O, C, N.

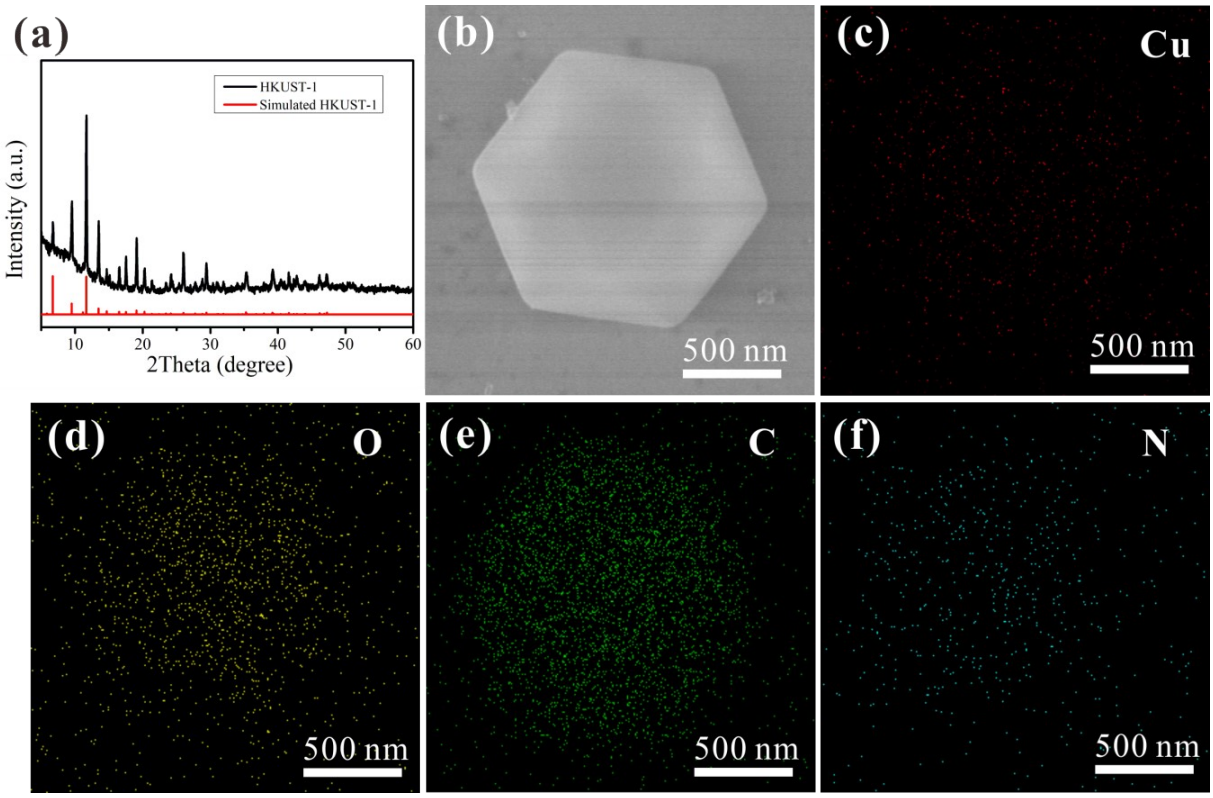

Fig. S2. (a) XRD pattern of the In-HKUST-1, (b,c)SEM image of the as-obtained In-HKUST-1, (d-h) the correspondingEDX elemental mapping of Cu, In, O, C, N.

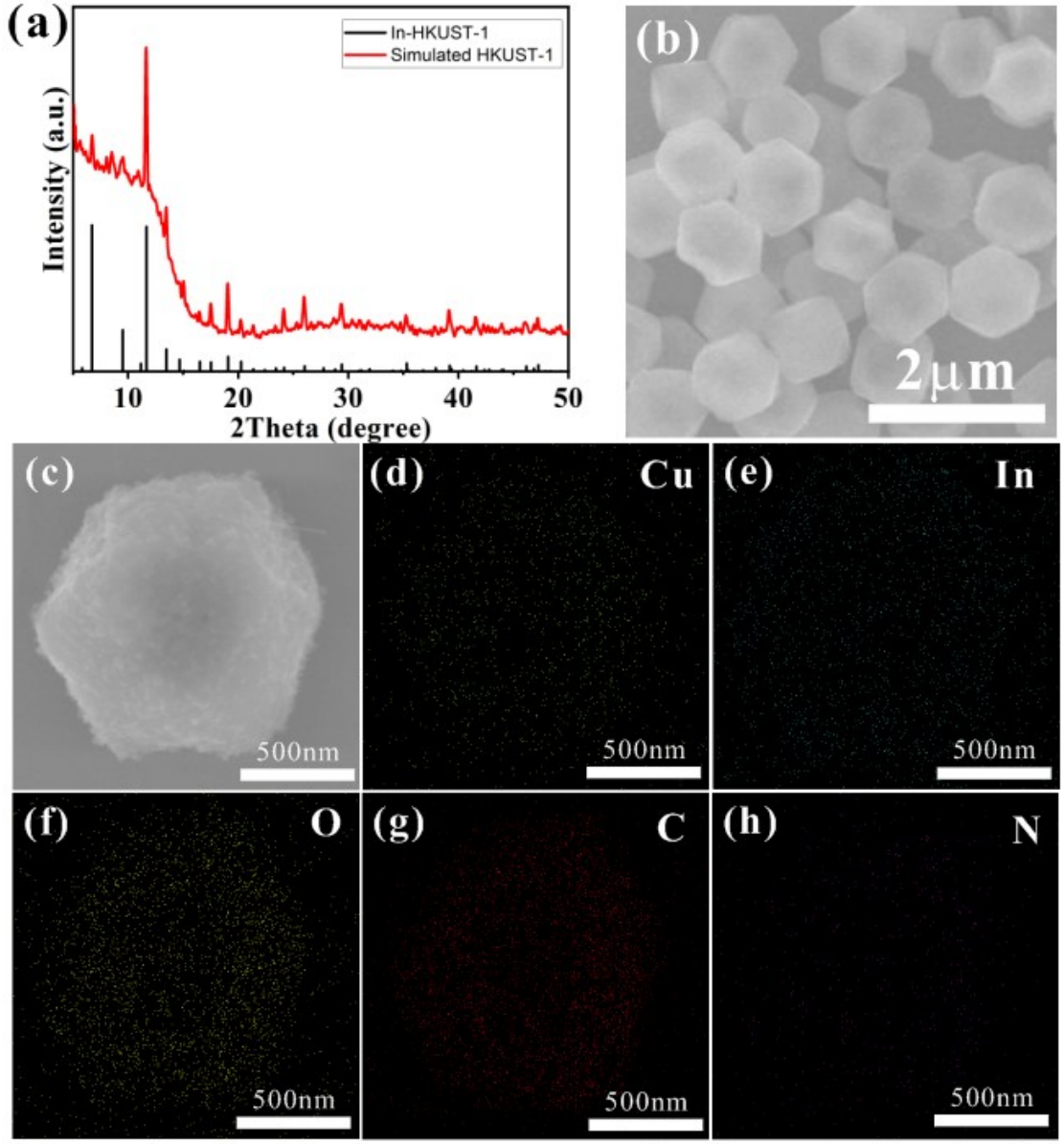

Fig. S3.TGA curves of the as-obtained In-HKUST-1 precursor.

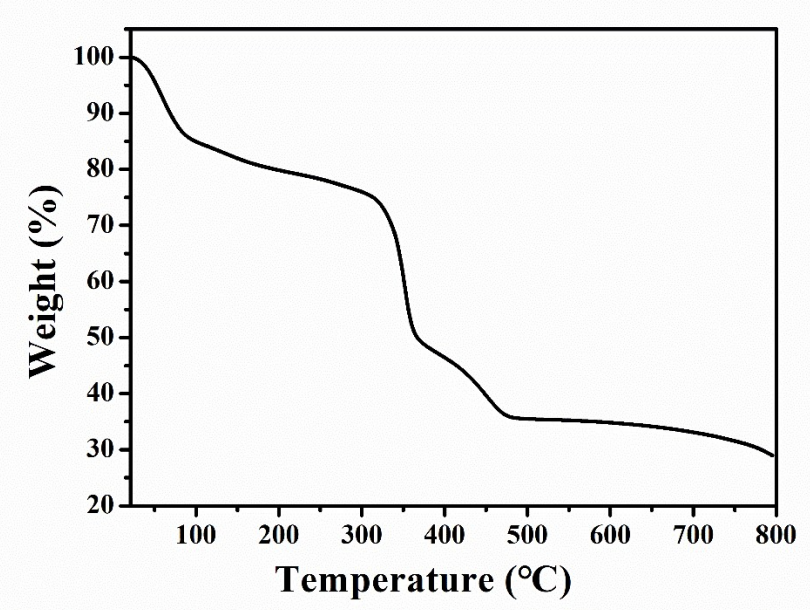

Fig. S4. The corresponding selected-area electron diffraction (SAED) of Cu/In_2O_3@N-C.

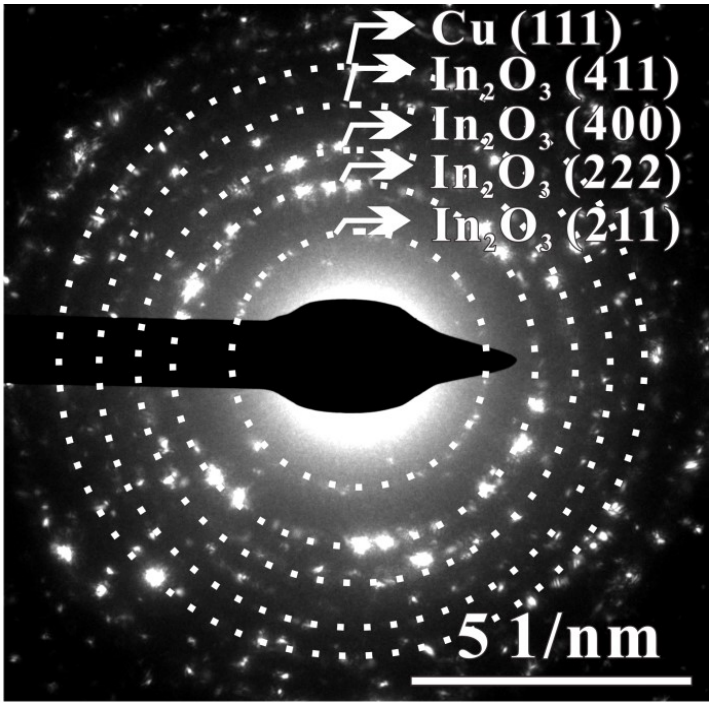

Fig. S5. (a) XRD pattern of Cu/In_2O_3@N-C, (b) Raman spectrum of Cu/In_2O_3@N-C

irradiated by 532 nm wavelength, (c) surface adsorption curve of Cu/In_2O_3@N-C (inset: pore size distribution).

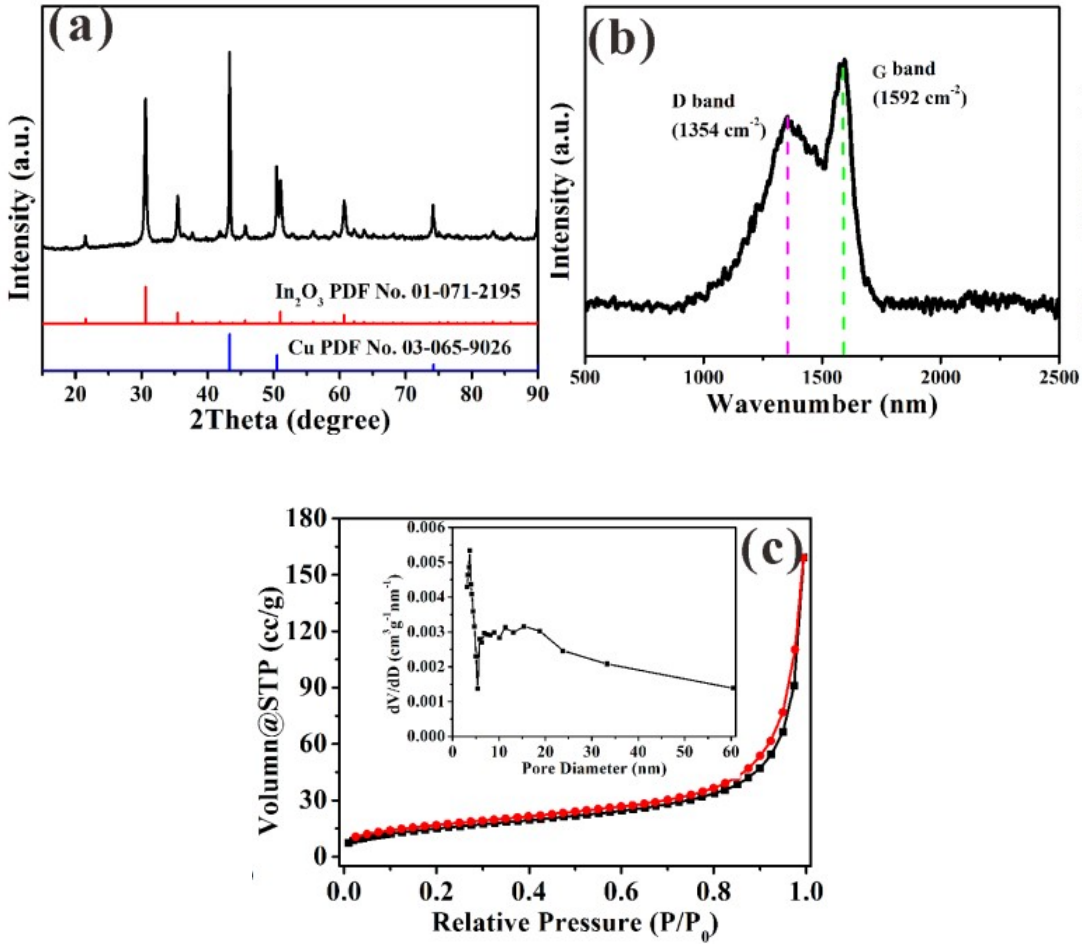

Fig. S6. Auger Cu LMM peak of Cu/In_2O_3@N-C nanocomposites.

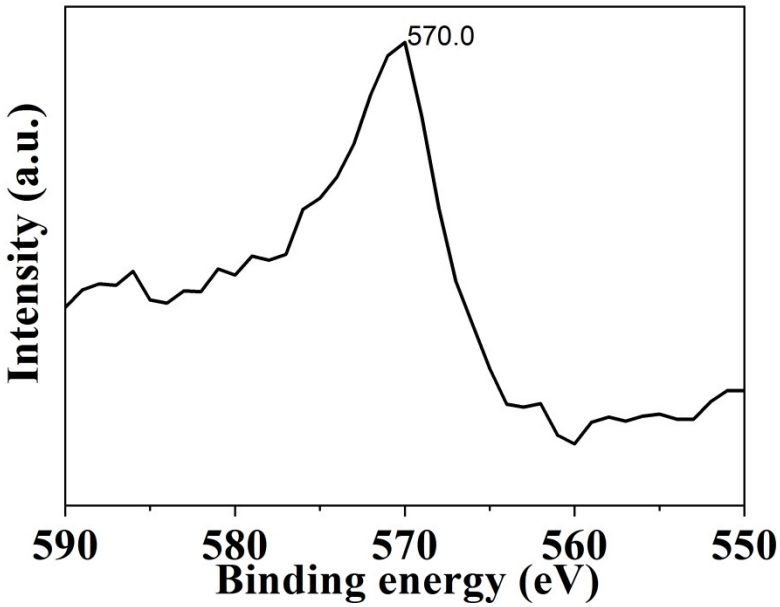

Fig. S7. (a)Typical XRD pattern of Cu/N-C, (b) SEM image of Cu/N-C, (c-f) corresponding

elemental mapping.

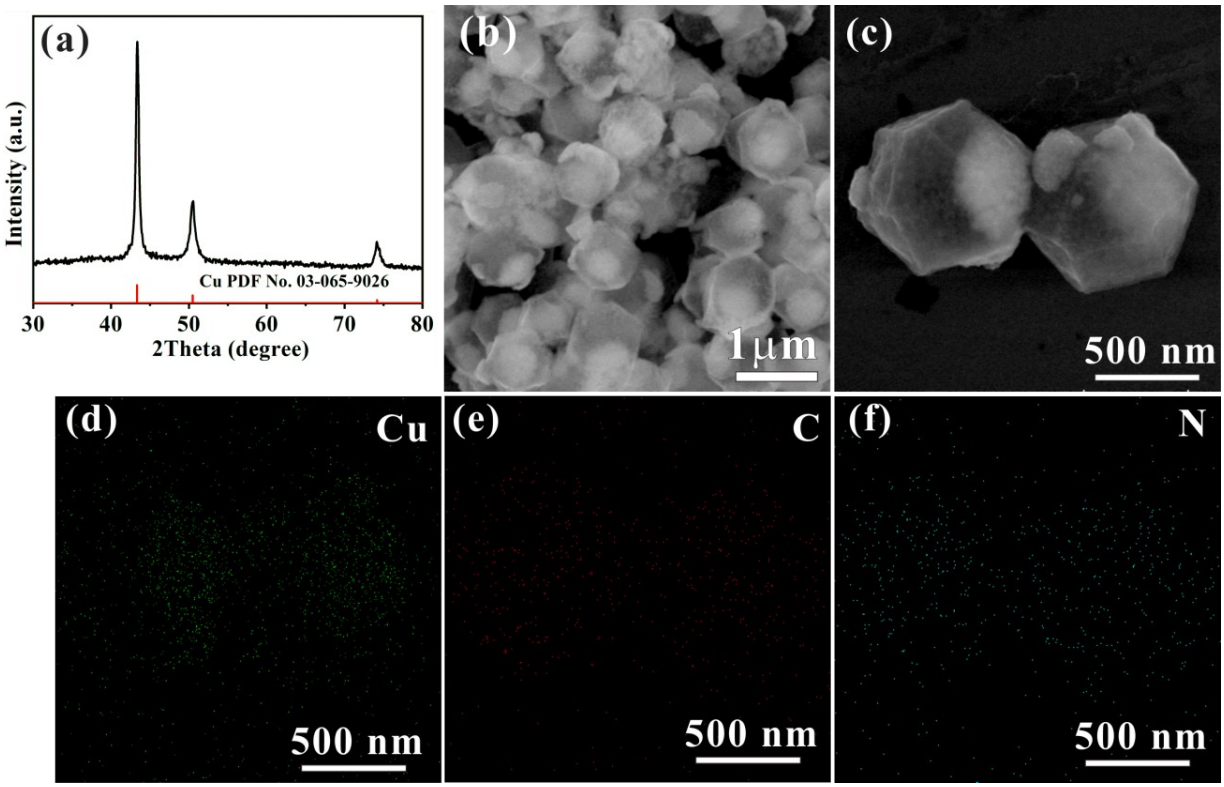

Fig. S8. (a)Typical XRD pattern of Cu/In_2O_3, (b) SEM image of Cu/In_2O_3, (c-h)

corresponding elemental mapping.

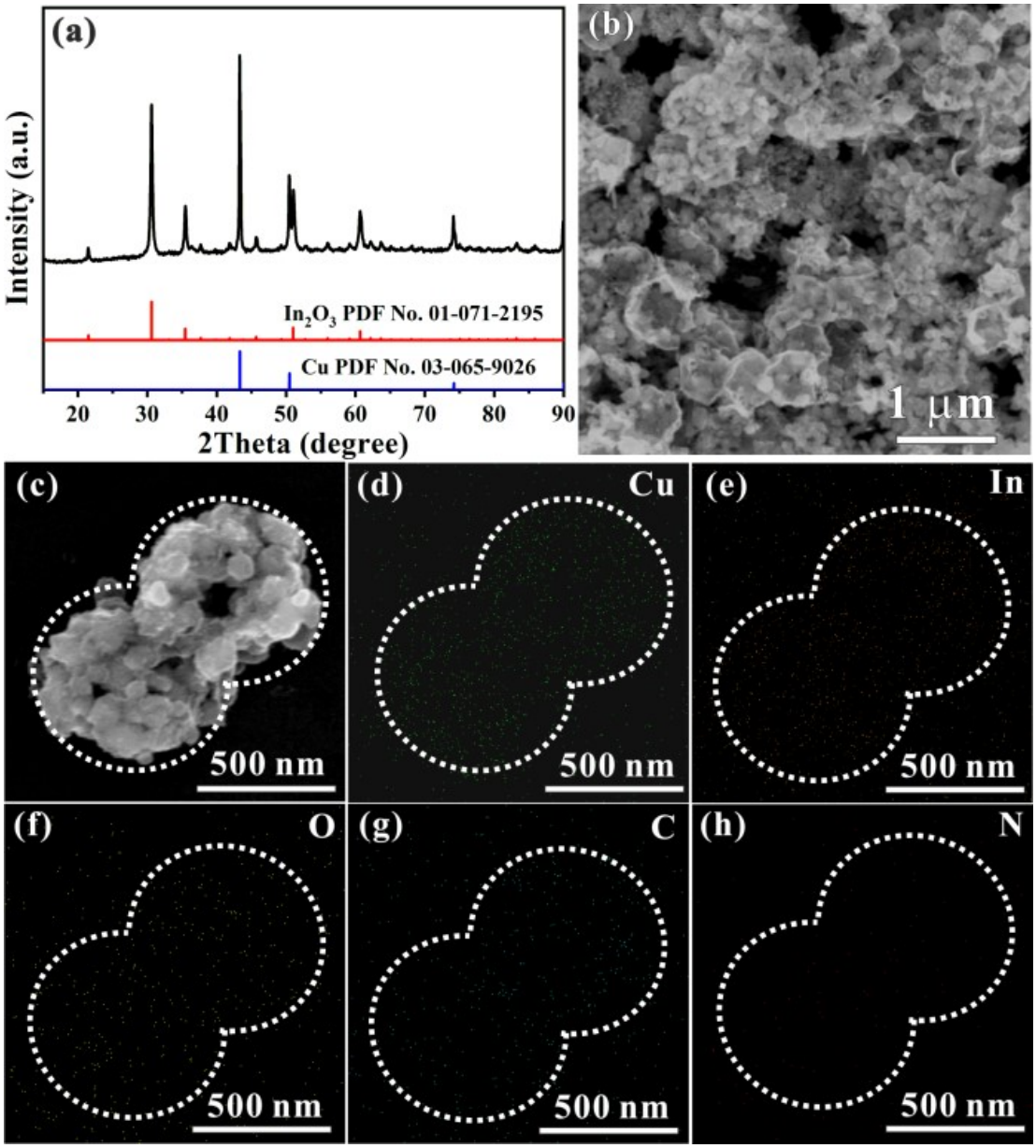

Fig. S9. XRD pattern of MOF precursor of In_2O_3@N-C (In-MOF), comparing with the

simulated data from ref [1].Their structures are almost the same.

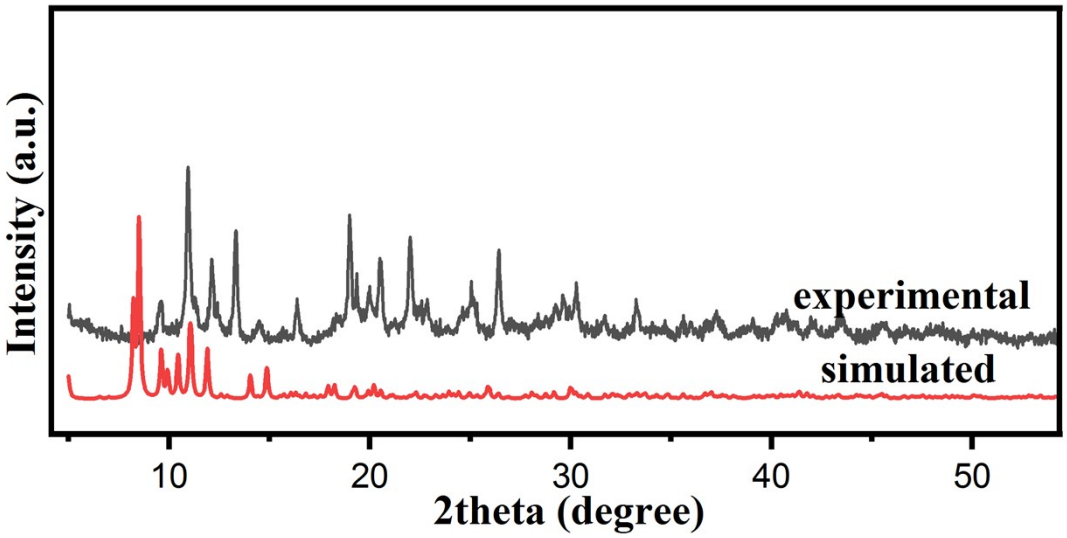

Fig. S10. (a) Typical XRD pattern of In_2O_3@N-C, (b) SEM image of In_2O_3@N-C, (c-h) corresponding elemental mapping.

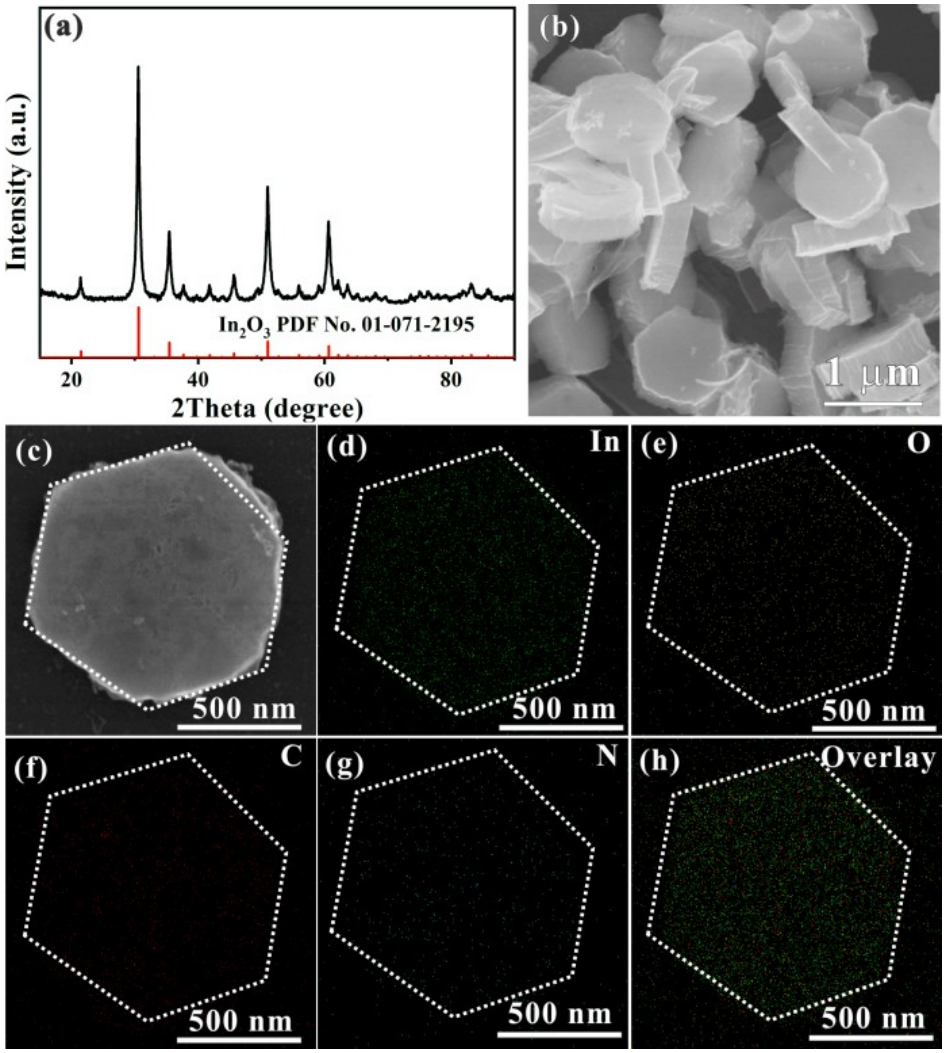

The calculation equation of the product yield:

$$yield = \frac{\frac{S_a}{2}}{\frac{S_a}{2} + S_c * 2} * 100\% \quad ,S_b = 2S_c, \text{Equation1}$$

S is the peak area of the corresponding peak.

Fig. S11. ^{1}H NMR spectrum of the product of homo-coupling of terminal alkynes for the four catalysts (a) Cu/In_2O_3@N-C, (b) Cu@N-C, (c) Cu/In_2O_3, (d)In_2O_3@N-C.

(a) Cu/In_2O_3@N-C

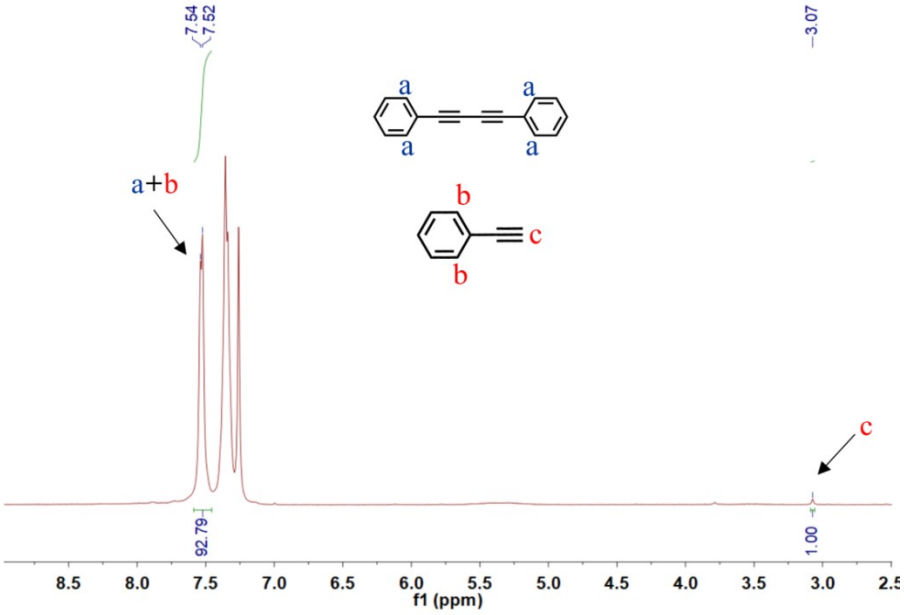

(b) Cu@N-C

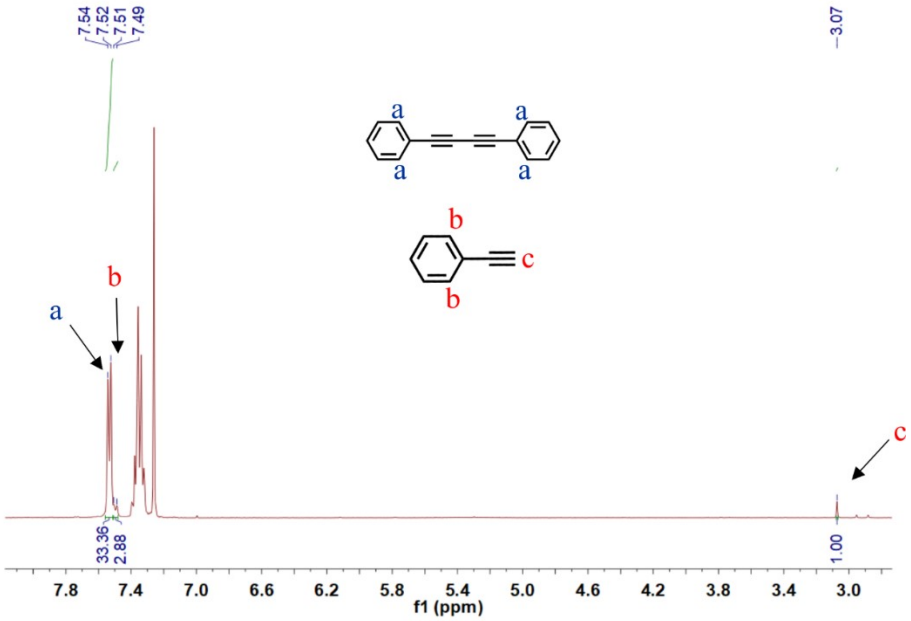

(c) Cu/In_2O_3

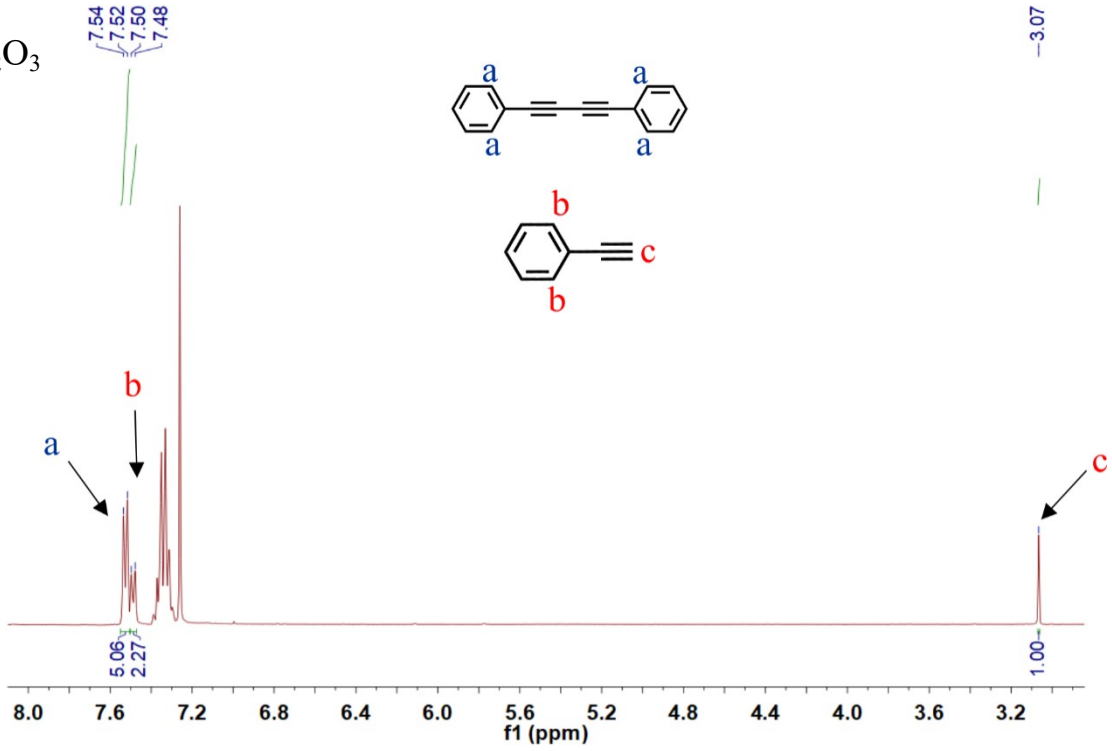

(d) In_2O_3@N-C

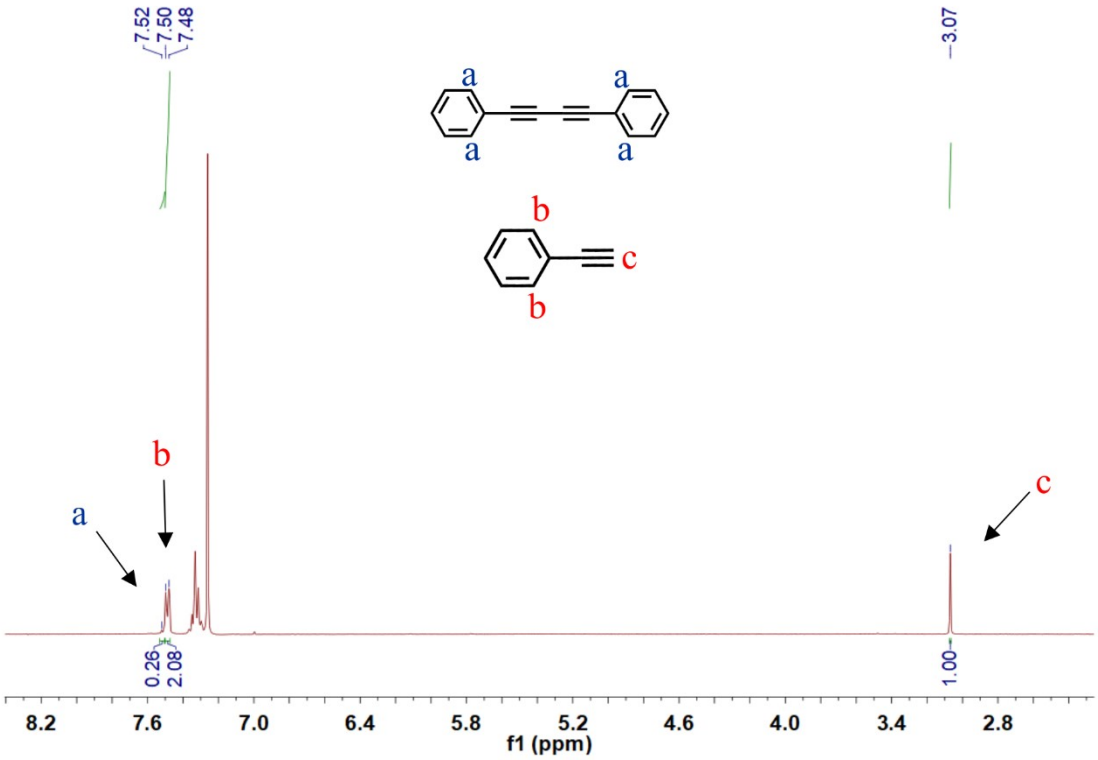

Fig. S12. Turnover frequency (TOF) graph of four catalysts.

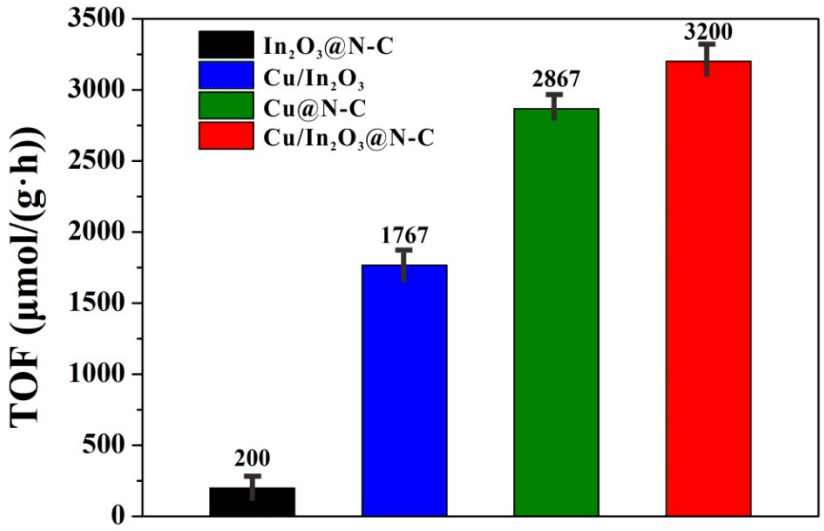

Fig. S13. Characterizations of Cu/In_2O_3@N-Cafter catalytic reaction (a) XRD pattern, (b) SEM image, (c) SEM image of single particle, (d-h) corresponding elemental mapping.

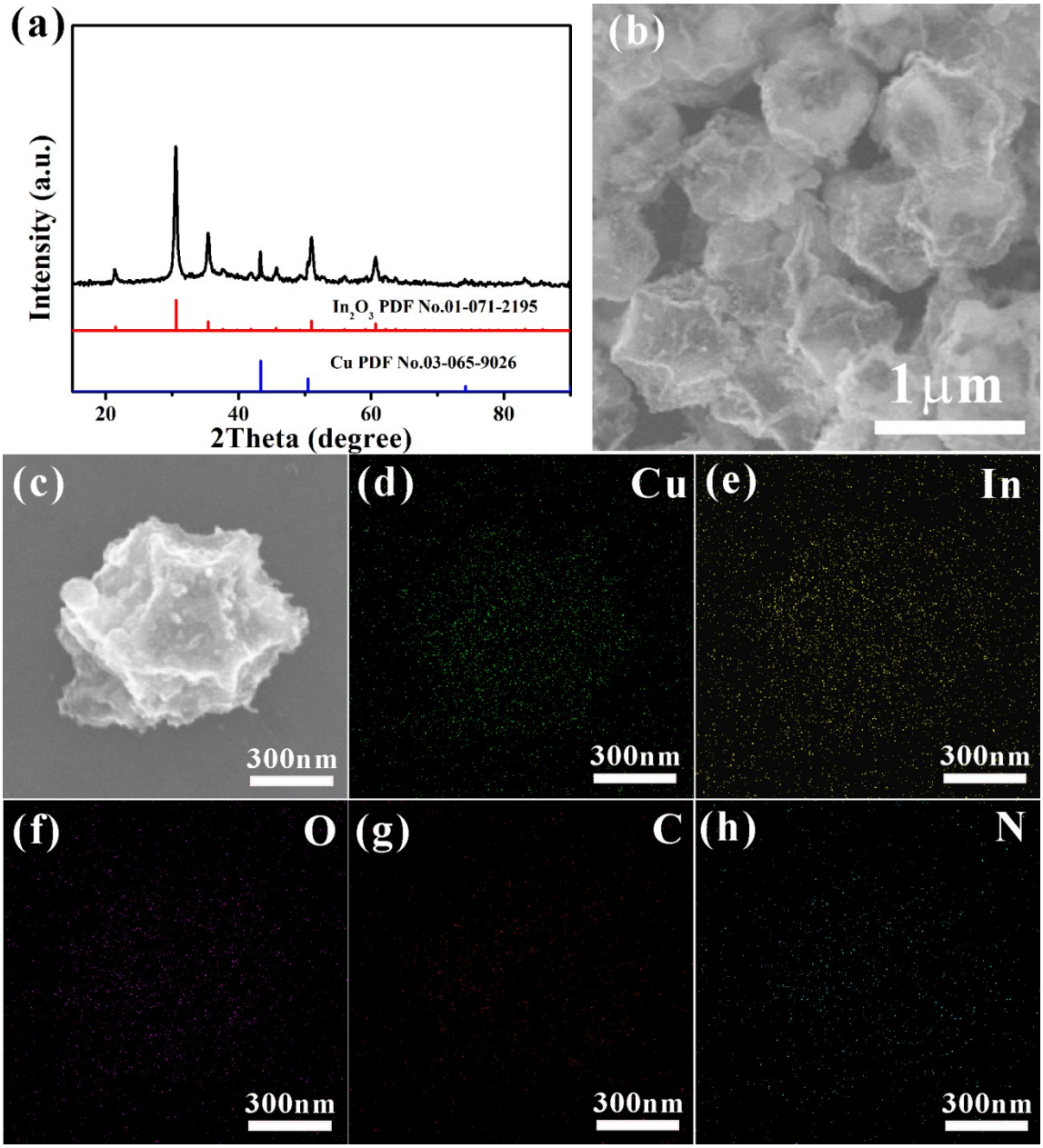

Fig. S14. Comparison of XRD pattern before and after catalytic reaction.

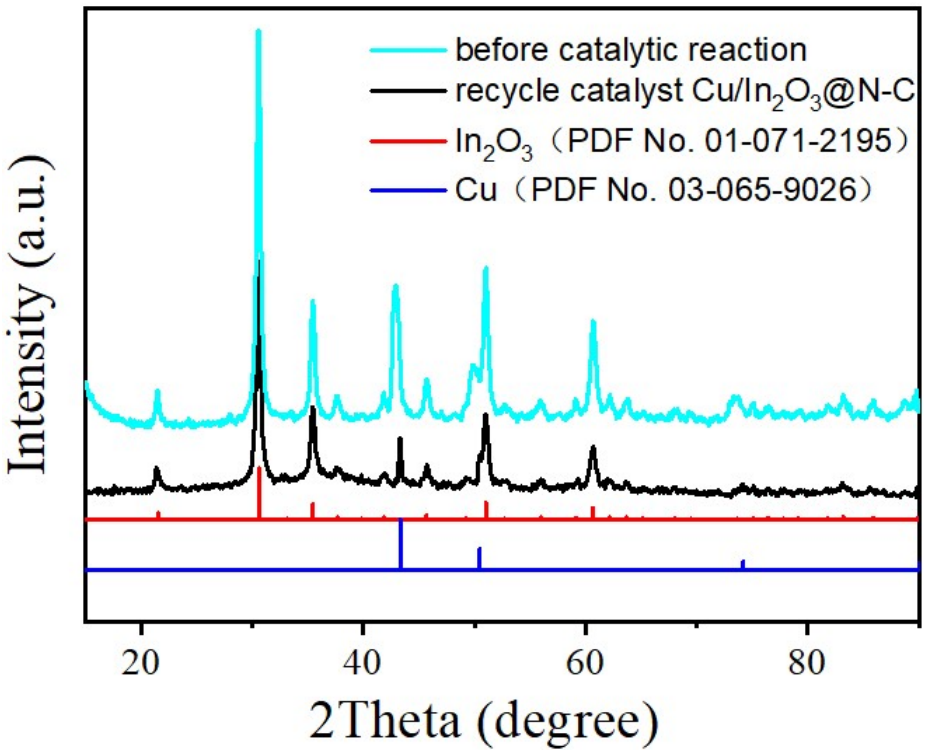

Fig. S15. Comparison of the photocatalytic efficiency of for aerobic oxidative coupling reaction of phenylacetyleneunder different wavelength of light.

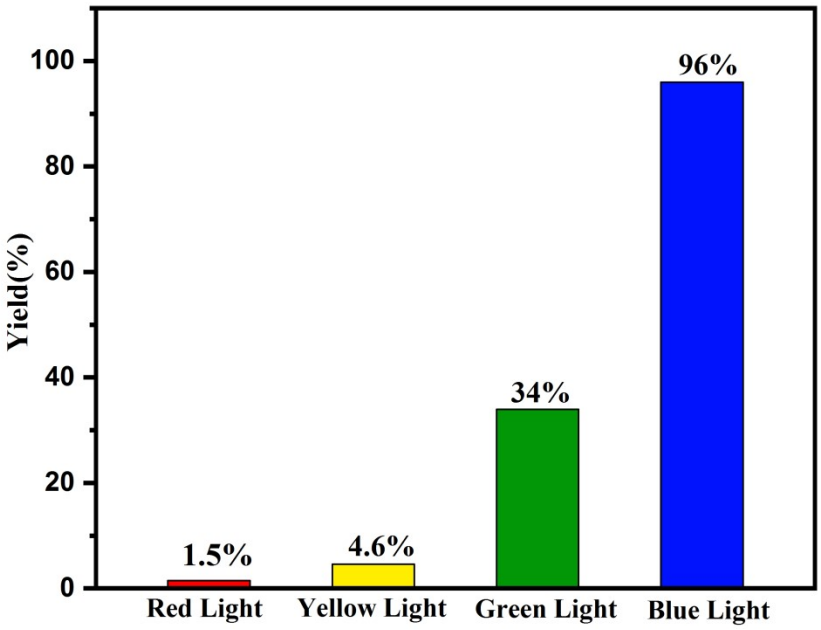

Literature survey

Table S1 The reported catalytic conditions for homo-coupling of terminal alkynes.

Ref[2]	[Cu][a]	Cu? [b]	Solvent	Temp	Oxidant	time	Conv.(%)
Cu-Cu_2O-C	1.65	Cu^0,Cu^+	CH_3CN	25, white LED	CO_2	20 h	>99
Entry	**Conv.(%)**	**Entry**	**Conv.(%)**	**Entry**	**Conv.(%)**	**Entry**	**Conv.(%)**
dark	7	Cu	c	Cu−Cu_2O−RGO	39	Cu-C	c
O_2	12	Cu_2O	2	Cu−Cu_2O−SWCNTs	18		
N_2	4	Cu Cu_2O	11	Cu−Cu_2O−graphite	15		
Ref [3]	[Cu]	Cu	Solvent	Temp	Oxidant	time	Conv.(%)
Cu/C_3N_4	10	Cu^0	iPrOH	25, KOH	O_2	6 h	99
Entry	**Conv.(%)**	**Entry**	**Conv.(%)**	**Entry**	**Conv.(%)**	**Entry**	**Conv.(%)**
CuNPs	69	$Cu(OAc)_2$	54	dark	99	H_2O	Trace
Neat	70	EtOH	15	iPrOH (2 eq.)	84	DMSO	15
Toluene	Trace	DMF	40	iPrOH (4 eq.)	99	CH_3CN	10
Substitute scope	Electron donating and withdrawing groups –good yields, but aliphatic alkyens worse						
Ref	[Cu]	Cu	Solvent	Temp	Oxidant	time	Conv.(%)
CuAl–hydro[4]	**110**	Cu^{2+}	CH_3CN	**25,TMEDA**	air	**4 h**	**88**
Fibe-PQN@Cu(I)[5]	**1**	Cu^+	**AcOEt**	**25,1-Butylamine**	air	**8 h**	**99**
SILP[6]	**6**	Cu^{2+}	CH_3CN	**25,TMEDA**	air	**4 h**	**88**
Ref	[Cu]	Cu	Solvent	Temp	Oxidant	time	Conv.(%)
Cu/TiO_2[7]	5	Cu^0	THF	65,piperidine	air	6 h	>99
Entry	**Conv.(%)**	**Entry**	**Conv.(%)**	**Entry**	**Conv.(%)**	**Entry**	**Conv.(%)**
Cu/activated C	9	zeolite Y	6	MgO	3	Al_2O_3	24
magnetite	91	H_2O	4	toluene	0	MeCN	0
EtOH	0	DMSO	0	acetone	0		
Ref	[Cu]	Cu	Solvent	Temp	Oxidant	time	Conv.(%)
Cu/TiO_2-D[8]	0.15	Cu^+	toluene	110	air	3 h	99
Entry	**Conv.(%)**	**Entry**	**Conv.(%)**	**Entry**	**Conv.(%)**	**Entry**	**Conv.(%)**
SF(Cu^{2+})	**20**	IMP(Cu^{2+})	**15**				
Ref	[Cu]	Cu	Solvent	Temp	Oxidant	time	Conv.(%)
Cu(OH)x/TiO_2[9]	**5**	Cu^{2+}	Toluene	**100**	O_2	**0.5 h**	**90-82**
Ref	[Cu]	Cu	Solvent	Temp	Oxidant	time	Conv.(%)
Cu(OH)x/ OMS-		Cu^{2+}	Toluene	100	O_2	10 min	98
CuOx/OMS-2[11]		Cu^{2+}	Toluene	100	air	12 h	98
Cu/MnOx[12]	6	Cu^{2+}	toluene	105	air	3 h	>99
N_2	70%						
Ref	[Cu]	Cu	Solvent	Temp	Oxidant	time	Conv.(%)
Cu-hydro[13]	15	Cu^{2+}	CH_3CN	reflux	air	72	98
CuNPs[14]	400	Cu^0	THF	66	air	8 h	90
CuNPs/MagSilica[15]	7.5		THF	66,piperidine	air	2 h	95
Cu(II)-clay[16]	10	Cu^{2+}	DMSO	80	O_2	3 h	98
Entry	**Conv.(%)**	**Entry**	**Conv.(%)**	**Entry**	**Conv.(%)**	**Entry**	**Conv.(%)**
CuNi/clay	53	CuMn/clay	53	CuZn/clay	61	CuAl/clay	58
CuFe/clay	39	CuSn/clay	62	CuO	34	Cu_2O	43
CuCo/clay	65						
Ref[17]	[Cu]	Cu	Solvent	Temp	Oxidant	time	Conv.(%)
CuCl	5	Cu^+	CH_3CN	25, blue LED	O_2	7 h	98
Entry	**Conv.(%)**	**Entry**	**Conv.(%)**	**Entry**	**Conv.(%)**	**Entry**	**Conv.(%)**
$CuCl_2$	c	$Cu(OAc)_2$	c	neat	c	MeOH	74
THF	23	DMSO	22	DMF	45	dark	c
Ref[18]	[Cu]	Cu	Solvent	Temp	Oxidant	time	Conv.(%)

$Cu(OAc)_2$	0.2	Cu^{2+}	DMSO	90	air	3	96
Entry	**Conv.(%)**	**Entry**	**Conv.(%)**	**Entry**	**Conv.(%)**	**Entry**	**Conv.(%)**
Cu tartrate	20	$CuSO_4$	67	CuC_{l2}	38	$CuBr_2$	46
Cu2citrate	28	$Cu(acac)_2$	42	$Cu(NO_3)_2$	30	CuO	c
1,4-Dioxane	56	MeCN	43	DMF	94	Toluene	c
Substitute scope	Electron donating –smooth yields and withdrawing groups –bad yields, but aliphatic						

Ref	**[Cu]**	**Cu**	**Solvent**	**Temp**	**Oxidant**	**time**	**Conv.(%)**
Cu_2-Sili[19]	4.4	Cu^{2+}	PhCN	100	O_2	3 h	91
Gold Clusters[20]							
Au-OMS-2[21]							
Au@CrADC[22]							

[a]**(mol %);**[b]**valencestate**

3. Computational Details

All density functional calculations were carried out utilizing Vienna ab-initio Simulation

Package (VASP).[23, 24]Within the framework of gradient of electronic density, Perdew Burke Ernzerhof (PBE)[25] functional was used to treat the exchange and correlation (XC) part in the Kohn−Sham equation. The ion-electron interaction was described by the projector-augmented wave (PAW)[26] pseudopotential, having the greater computational efficiency of plane wave as well as high accuracy of ultrasoft pseudopotential. Plane wave function with kinetic energy less than E_{cut} of 450 eV is included in the basic set. The K-Point mesh of 4 × 4 ×2 grid, featuring enough accuracy to total energy by convergence test, was used to sample Brillouin zone for geometrical optimization. For self-consistent field (SCF) calculations, the stopping criterion was set to the energy difference less than 1.0×10^{-5} eV, while for geometrical optimization the convergence will reach until the Hellmann−Feynman force per atom less than 0.01 eV/Å. Moreover, DFT-D3BJ[27]method was used to correct the Van der Waals force. The adsorption energy is typically evaluated as following formula: E_a= E(phenylacetylene/Cu/In_2O_3) – E(phenylacetylene) – E(Cu/In_2O_3), where E(phenylacetylene/Cu/In_2O_3), E(phenylacetylene) and E(Cu/In_2O_3) are single-point energy of relaxed configurations.

Fig. S16. Total density of states of Cu/In_2O_3 with the charge density of VBM and CBM.

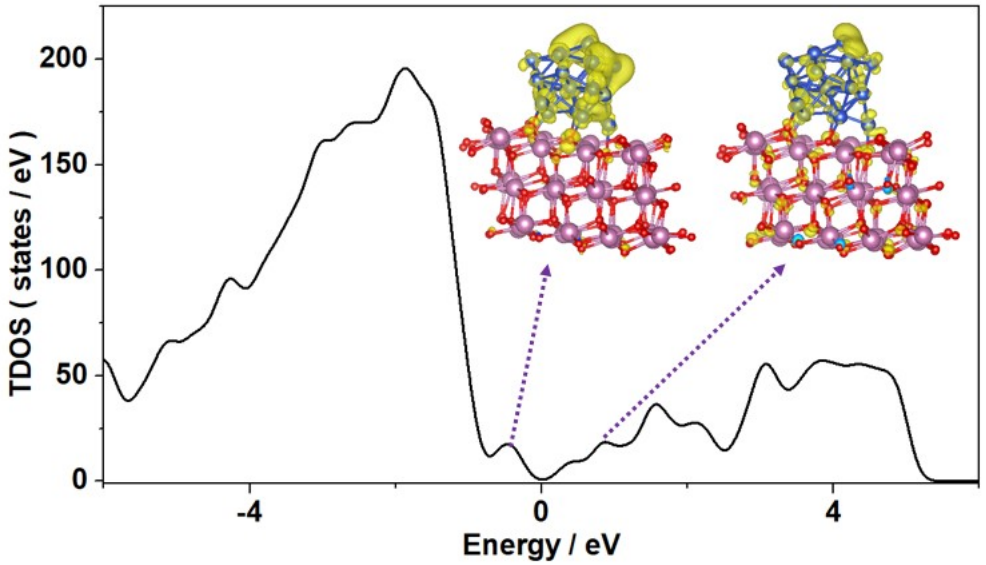

Fig. S17. Partial density of states of Cu/In_2O_3.

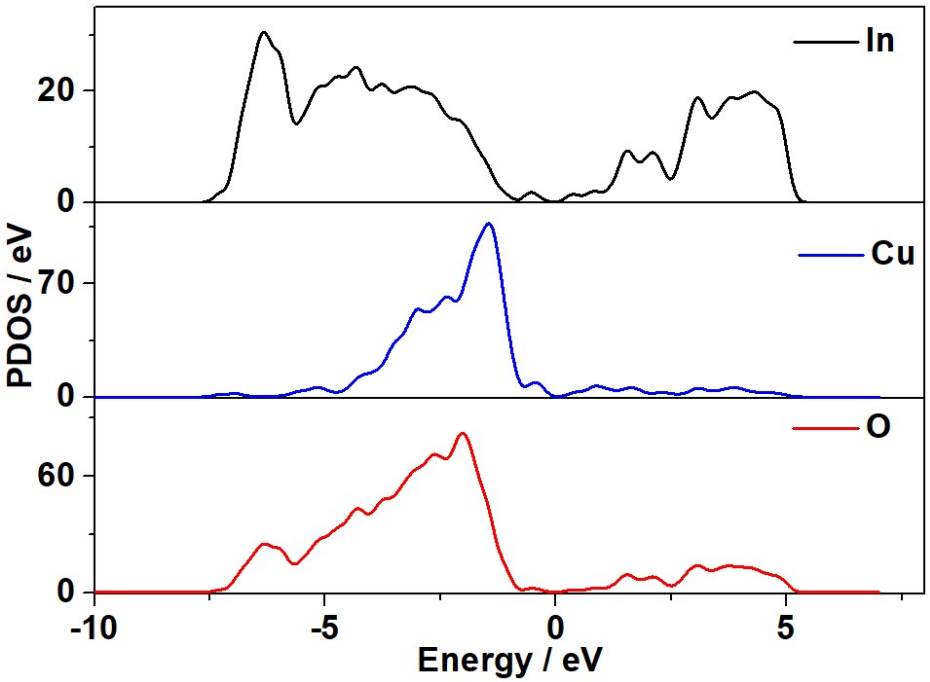

Fig. S18. Adsorption structure of phenylacetylene on Cu/In_2O_3 with two side view.

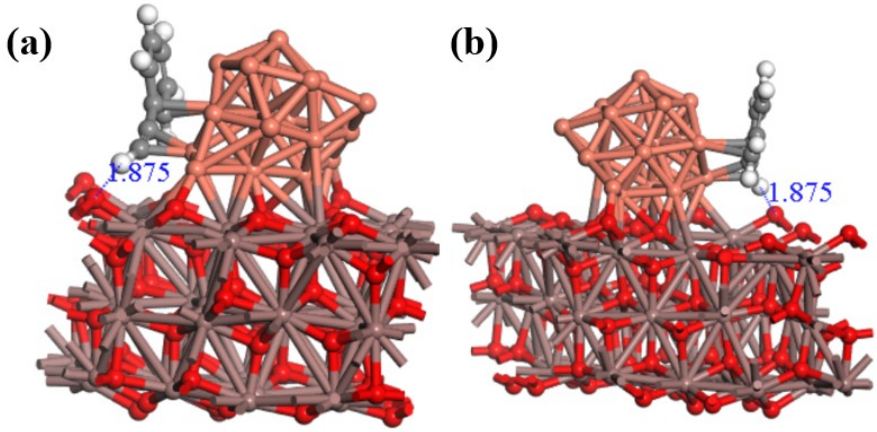

4. References

1 S. T. Zheng, J. T. Bu, Y. Li, T. Wu, F. Zuo, P. Feng and X. Bu, *J. Am. Chem. Soc.*, 2010, **132**, 17062-17064.

2 J. Cai, Y. Li, M. Zhang and Z. Li, *Inorg. Chem.*, 2019, **58**, 7997-8002.
3 H. Xu, K. Wu, J. Tian, L. Zhu and X. Yao, *Green Chem.*, 2018, **20**, 793-797.
4 B. C. Zhu and X. Z. Jiang, *Appl. Organomet. Chem.*, 2007, **21**, 345-349.
5 Q. Hu, X.-L. Shi, Y. Chen, F. Wang, Y. Weng and P. Duan, *J. Ind. Eng. Chem.*, 2019, **69**, 387-396.
6 S. Normen, *Comb. Chem. High Throughput Screening*, 2012, **15**, 170-179.
7 F. Alonso, T. Melkonian, Y. Moglie and M. Yus, *Eur. J. Org. Chem.*, 2011, **2011**, 2524-2530.
8 Z. Luo, S. A. Cetegen, R. Miao, T. Jiang, S.-Y. Chen, T. Jafari, Y. Zhang and S. L. Suib, *J. Catal.*, 2016, **338**, 94-103.
9 T. Oishi, T. Katayama, K. Yamaguchi and N. Mizuno, *Chem. Eur. J.*, 2009, **15**, 7539-7542.
10 T. Oishi, K. Yamaguchi and N. Mizuno, *ACS Catal.*, 2011, **1**, 1351-1354.
11 Y. Huang, K. Zheng, X. Liu, X. Meng and D. Astruc, *Inorg. Chem. Front.*, 2020, **7**, 939-945.
12 S. Biswas, K. Mullick, S.-Y. Chen, D. A. Kriz, M. D. Shakil, C.-H. Kuo, A. M. Angeles-Boza, A. R. Rossi and S. L. Suib, *ACS Catal.*, 2016, **6**, 5069-5080.
13 B. Maaten, J. Moussa, C. Desmarets, P. Gredin, P. Beaunier, T. Kanger, K. Tõnsuaadu, D. Villemin and M. Gruselle, *J. Mol. Catal. A: Chem.*, 2014, **393**, 112-116.
14 G. Radivoy, F. Nador, L. Fortunato, Y. Moglie and C. Vitale, *Synthesis*, 2009, **2009**, 4027-4031.
15 F. Nador, M. A. Volpe, F. Alonso, A. Feldhoff, A. Kirschning and G. Radivoy, *Appl. Catal. A Gen.*, 2013, **455**, 39-45.
16 B. A. Dar, D. Vyas, V. Shrivastava, S. Farooq, A. Sharma, S. Sharma, P. R. Sharma, M. Sharma and B. Singh, *C. R. Chimie*, 2014, **17**, 316-323.
17 A. Sagadevan, V. P. Charpe and K. C. Hwang, *Catal. Sci. Technol.*, 2016, **6**, 7688-7692.
18 X. Jia, K. Yin, C. Li, J. Li and H. Bian, *Green Chem.*, 2011, **13**, 2175-2178.
19 K. Kamata, S. Yamaguchi, M. Kotani, K. Yamaguchi and N. Mizuno, *Angew. Chem.*, 2008, **120**, 2441-2444.
20 B. Vilhanová, J. Václavík, L. Artiglia, M. Ranocchiari, A. Togni and J. A. van Bokhoven, *ACS Catal.*, 2017, **7**, 3414-3418.
21 K. Yamaguchi, Y. Wang, T. Oishi, Y. Kuroda and N. Mizuno, *Angew. Chem. Int. Ed. Engl.*, 2013, **52**, 5627-5630.
22 J. Chen, Y. Xin, J. Wu, P. Liao, L. Chen and J. Zhang, *ChemNanoMat*, 2021, **7**, 334-340.
23 G. Kresse and J. Furthmüller, *Comp. Mater. Sci.*, 1996, **6**, 15-50.
24 G. Kresse and J. Hafner, *Phys. Rev. B: Condens. Matter*, 1993, **47**, 558-561.
25 J. P. Perdew, K. Burke and M. Ernzerhof, *Phys. Rev. Lett.*, 1996, **77**, 3865-3868.
26 P. E. Blochl, *Phys. Rev. B: Condens. Matter*, 1994, **50**, 17953-17979.
27 H. Schroder, A. Creon and T. Schwabe, *J Chem Theory Comput*, 2015, **11**, 3163-3170.